Wind-Tunnel Tests and Computer Simulations of Buoyant Wing-Tip Vortices

R.C. Costen,* R.E. Davidson,*
NASA Langley Research Center, Hampton, Va.
and
G.T. Rogers†
Union Carbide Corp., Florence, S.C.

Wind-tunnel tests have demonstrated that buoyant fluid ejected downstream at a wing-tip or flap-tip will enter the core of the trailing vortex and cause it to drift horizontally in accordance with the theory for buoyant-core vortices. This result indicates that locating the propulsion engines of a jet aircraft at the wing-tips and/or flap-tips would cause the vortices from the two wings to drift toward each other as they descend, and thus break up more quickly through the Crow or burst instability. Two-dimenslonal computer simulations showed that engine placement is critical because distributed buoyancy resulting from general engine placement or from descent of the wake in a stable atmosphere does not promote this drift.

Introduction

BUOYANT vortices are of interest in aerodynamics because the wing-tip vortices generated by an aircraft can become buoyant by heating from the jet exhaust or by descending in a stable atmosphere, and this buoyancy can affect their persistence. According to a theoretical treatment by Costen,[1] a vortex with a buoyant core drifts so that the Magnus force generated by the drift balances the transverse component of the Archimedian force. If the jet engine exhaust were concentrated in the cores of the wing-tip vortices, they would drift toward each other as they descend; this drift should expedite their breakup through the Crow[2] instability or the burst instability, as photographed for aircraft wakes by Tombach.[3]

The purpose of this research is to show that buoyant-core vortices generated in a wind tunnel drift toward each other as predicted. Two-dimensional computer cimulations are used to explain why distributed buoyancy resulting from general engine placement, or from descent of the wake in a stable atmosphere, does not have the same effect.

Other methods that have been proposed for dissipating aircraft wakes include varying the wing loading (Chevalier,[3] Crow,[4] Bilanin and Widnall,[5] Ciffone and Orloff,[6] and Corsiglia, Rossow, and Ciffone[7]) blowing into the vortex cores (Poppleton,[8] Mason and Marchman,[9] and White and Balcerak[10]), and placing obstacles in the vortex cores (Patterson,[11] and Zalovcik and Dunham[12]). The effectiveness of many of these methods could be improved by combining them with vortex core heating to take advantage of buoyant effects. For example, a problem with generating the Crow instability by oscillating inboard and outboard flaps (Crow,[4] and Bilanin and Widnall[5]) is that the Crow instability does not always go to completion. Core heating could bring the instability to completion by driving the inboard segments of the vortices together.

Presented at the AMS/AIAA Sixth Conference on Aerospace and Aeronautical Meteorology, El Paso, Tex., November 12-14, 1974; submitted December 26, 1974; revision received October 22, 1975. The authors acknowledge the help of L.M. Weinstein, D.R. Croom, and S. Katzoff of Langley Research Center in making the wind tunnel tests.

Index categories: Jets, Wakes, and Viscid-Inviscid Flow Interactions; Aircraft Configuration Design; Hydrodynamics.

*Aerospace Technologists, Analytical Studies Branch, Space Applications and Technology Division.

†Product Design Engineer, Product Engineering Department.

Wind-Tunnel Studies of Buoyant Wing-Tip Vortices

Wind-Tunnel Setup

The wind-tunnel experiments were performed at the V/STOL Model Tunnel at NASA Langley Research Center. This is a small wind tunnel with a semi-open test section of dimensions 0.51-m width × 0.76-m height × 1.75-m length. A 0.152-m semispan wing was mounted horizontally from the sidewall of the section which acted as a reflection plane for the other half of the wing, as shown in Fig. 1. The wing section was type NACA 0012 with a chord of 9.31-cm. Tests were made at attack angles $\alpha = 9°$, 12° (clean wing), and $\alpha = 6°$ (flapped wing). The flap was a 2.54-cm sealed full flap attached to the trailing edge and deflected 30° from the wing-section center line. The corresponding lift coefficients C_L are given in Fig. 2.

The tip vortex was made buoyant by piping helium through a 7.94-mm i.d. tube runing spanwise within the wing and ejecting it downstream at the wing-tip. The flow of helium was measured with a helium flowmeter and corrections were made for the pressure in the line at the flowmeter. The tube was shaped so that the helium was always ejected horizontally downstream from the wing-tip (or flap-tip). For the flapped wing, therefore, the tube formed a partial end plate at the wing-tip, as shown in Figs. 2c to 2e. Besides the 7.94-mm exit orifice of the tube, two 7° screened diffusers were made for attachment to the end of the tube to reduce the velocity of the helium jet by a factor of 4 and a factor of 10. The diffusers contained mutliple screens of mesh size 0.423-mm, as shown in Fig. 2, to prevent flow separation. Stagnation pressure tests verified that the helium flow was uniform over the exit orifice of each diffuser.

Transition to Turbulence

At 1.375-m downstream of the wing, the flow was viewed by a vertical schlieren system with a 0.152-m diameter circular field, as shown in Fig. 1. Flash schlieren photographs were made for various tunnel speeds, helium flow rates, and diffusers. Sample results from three runs are shown in Fig. 3. Since the schlieren system is sensitive to density gradients, the inboard half of the helium core appears white and the outboard half is black.

With no helium injection, the schlieren photographs showed only a uniform background. At small helium flows, a narrow, laminar helium core developed in the center of the vortex. Correspondence between the helium and the vortex

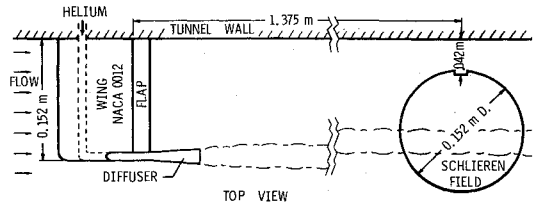

Fig. 1 Top view of wind-tunnel setup with wall-mounted semispan wing, helium piping, and schlieren system.

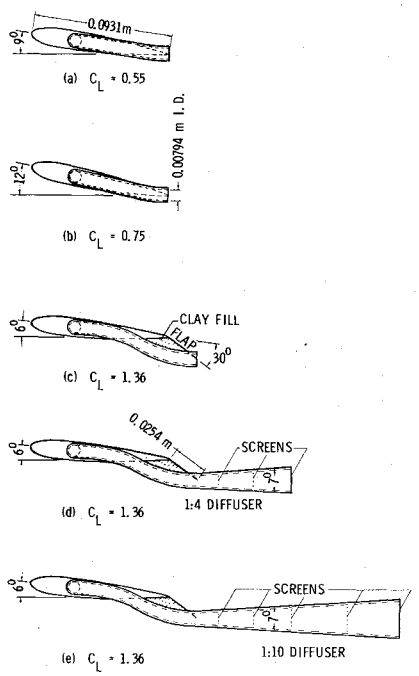

Fig. 2 Side views of the various wing and helium ejection configurations tested with the corresponding wing lift coefficients C_L.

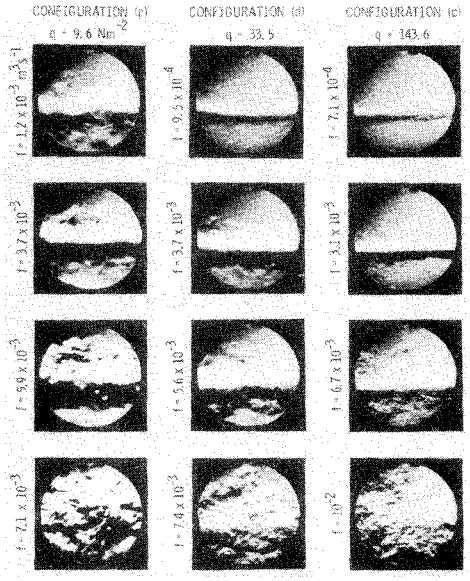

Fig. 3 Representative flash schlieren photographs from three tunnel runs. (For each run, the tunnel dynamic pressure q and wing configuration were fixed and the volumetric helium flux f was varied. The configuration designations refer to Fig. 2. The notch is near the tunnel wall, as shown in Fig. 1.

center was apparent from helical lines on the surface of the helium core in some of the original photographs, although these lines are not visible in the reproductions. Since the photographs were taken 1.375-m downstream of the wing, helium evidently was retained in the cores against the action of gravity by the radial pressure gradient in the vortex. (An additional run (not shown) was made with CO_2 instead of helium. Instead of remaining in the vortex core, the CO_2 spread across the 0.152-m schlieren field of view. This confirmed the expectation that gases heavier than air would be spun out of the vortex core.) As the helium flow increased, the size of the laminar helium core increased until, at sufficiently high helium flows, a transition to turbulence occurred over a region several times the diameter of the laminar core, and ultimately the flow became turbulent across the schileren field of view.

During these runs, a tuft grid with 2.54-cm interstices was positioned in the wake downstream of the schlieren system. The tuft grid showed that for small helium flows the vortex core was very small. As the helium flow increased, the vortex core diameter became larger until finally the core became very large and diffuse, in agreement with what the schlieren photographs indicated. (For the CO_2 runs, there was no correlation between the schileren photographs and the tuft grid, for at small CO_2 flows, the tuft grid showed that the vortex core was very small, while the schlieren photographs indicated that the CO_2 was widely dispersed.) The transition to turbulence shown in Fig. 3 is in qualitative agreement with reports by Poppleton,[8] Marchman and Mason,[9] and White and Balcerak.[10]

A formula for the volumetric transition flux of helium f_t was inferred from the tunnel runs

$$f_t = 0.08 \quad C_L (qA)^{1/2} \tag{1}$$

where C_L is the lift coefficient of the wing (including the reflected semi-span), q is the dynamic pressure of the wind-tunnel flow, and A is the area of the jet orifice. The jet velocity v_t^{jet} at transition is given by

$$v_t^{\text{jet}} = 0.08\, C_L (q/A)^{1/2} \tag{2}$$

From this formula, the ratio of total thrust F (from the jet and its image) to the induced drag D_i of the semispan and its reflection may be determined

$$\frac{F}{D_i} = 4.02 \times 10^{-2} \frac{\rho(He)}{c^2} = \begin{cases} 0.79 \text{ (clean wing)} \\ 0.51 \text{ (flapped wing)} \end{cases} \tag{3}$$

where $\rho(He)$ is the density of the helium jet, and c is the chord. Since the transition thrust is less than the induced drag, and since an aircraft's propulsion engines must develop substantially more thrust than the induced drag, it appears that transition can be induced by placing the engines at the wing-tips and/or flap-tips.

Drift of Buoyant-Core Vortex

Because of the short distance between the wing and the schileren field, the horizontal drift of the vortex due to buoyancy was measurable only at $q = 9.6$ N/m^2. The distance from the wall to the vortex center was obtained from the schileren photographs. A plot of this distance against the volumetric helium flux f is shown in Fig. 4. The scatter in the data is due to the Crow instability (kink instability), as evidenced by the vortex curvature in the top-center photograph of Fig. 3. The solid line in Fig. 4 minimizes the squared deviations. As shown, it lies much closer to the theoretical line derived from the drift formula given by Costen[1] than to the line of zero drift. We conclude that this drift formula is supported by the wind-tunnel experiments.

Computer Simulation of Buoyant Wing-Tip Vortices

Buoyant Fluid Concentrated in Vortex Cores

Aditional information on the interaction of buoyant wing-tip vortices in near proximity can be obtained from two-

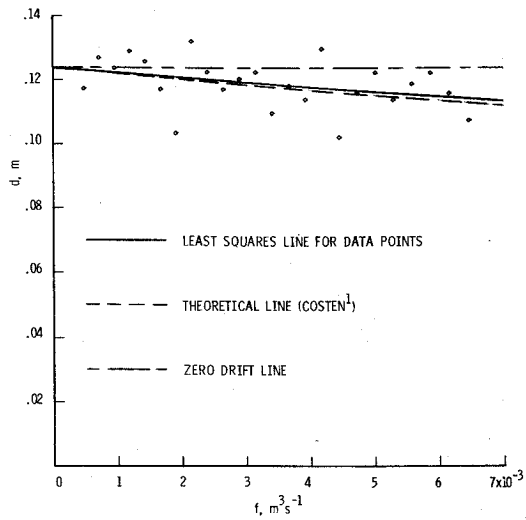

Fig. 4 Plot of distance d from tunnel wall to the axis of the wing-tip vortex within the schlieren field against volumetric helium flux f for tunnel dynamic pressure $q = 9.6\ N/m^2$ and wing configuration (e) of Fig. 2. The data points were obtained from flash schlieren photographs.

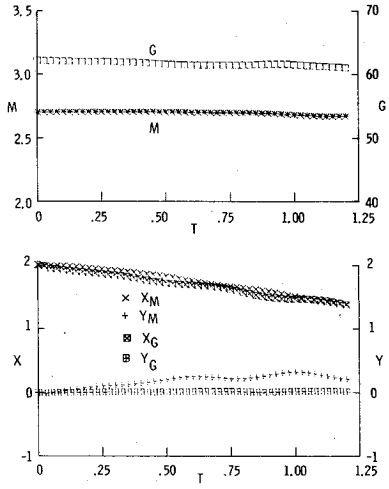

Fig. 5 Dimensionless cross-sectional plots of evolving density defect $1-R$, vorticity Ω, and velocity (U, V) for a wing-tip vortex with buoyant fluid concentrated in the core. Amplitude is indicated by the size of the dark squares and the size of the arrows. Gravity acts in the negative Y-direction, and the corresponding Archimedian force acts in the positive Y-direction. The symmetry plane is at $X=0$. The stagnation point at the vortex center is shown to drift from $X=2$ to $X=1.4$. The interval $T=1$ corresponds to one revolution of the fluid elements at unit radius from the vortex axis.

dimensional computer simulations made in a plane perpendicular to the vortex axes. The simulations are based on the continuity, momentum, and vorticity equations for an inviscid, incompressible fluid of nonuniform density subject to gravity. These equations are nondimensionalized and integrated for the evolution of the nondimensional density R, vorticity Ω, and velocity (U, V) on the nondimensional X-Y plane from a prescribed initial state.

An initial state ($T=0$) for buoyant-core vortices is shown in Fig. 5. Initially, the vorticity Ω and the density defect $1-R$ (which denotes the buoyant fluid) are superimposed Gaussian functions of the radius from the vortex center (2,0). Gravity acts in the negative Y-direction. The center-to-center distance of the vortices is four times their radius. The radius is nominally taken to be that where the amplitudes of the vorticity and the density defect fall off to e^{-1} times their central values. In the nondimensional coordinates (X, Y) this radius is unity.

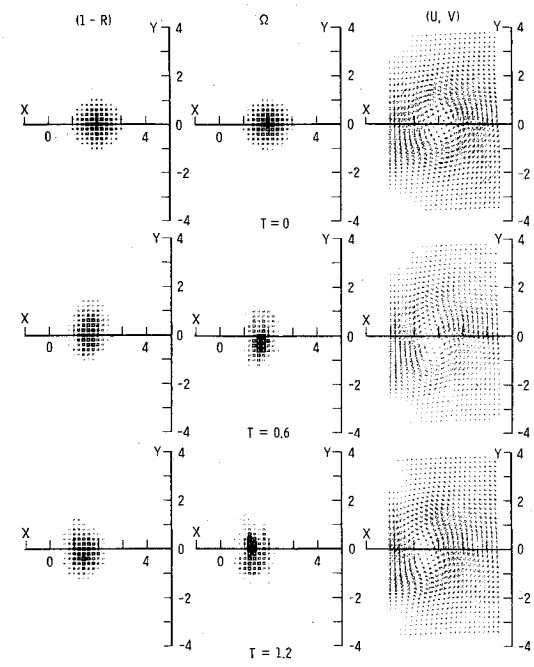

Fig. 6 Timewise variation of the dimensionless circulation G and mass defect M and the coordinates of their centroids for the buoyant-core vortex computation of Fig. 5.

The circulation and core diameter correspond to wing-tip vortices generated by the Boeing 747 aircraft. The computation starts, however, when the vortices are alreay fairly close together. The cores are filled with helium instead of jet engine exhaust in order to accelerate the drift and to allow the computation to be performed before numerical errors become significant.

Figure 5 shows that as time progresses, the vortices are driven toward each other by buoyant effects at a drift rate that agrees with the theory. The vortex cores become elongated as in the calculation by Pocklington[13] of hollow contra-rotating vortices in near proximity without gravity. The drift is also consistent with the Bjerknes equation as given by Lamb.[14] According to this equation, the vorticity decreases on the right-hand periphery of the buoyant core and increases on the left-hand periphery; consequently, the vortex is displaced while the total circulation remains constant.

The evolution of the dimensionless circulation G and mass defect M for the right-hand vortex is shown for this computation in Fig. 6. Also shown in this figure are the dimensionless coordinates (X_G, Y_G) for the centroid of circulation and (X_M, Y_M) for the centroid of mass defect. The waves on these curves correspond to internal oscillations of the centroids of circulation and mass defect, with both tracing trochoidal paths. During the computation, G and M remain essentially constant and their centroids drift in the negative X-direction (toward the image vortex). The adjusted upflow successfully kept $Y_G = 0$. The corresponding descent speed of the vortex pair, although not plotted in Fig. 6, was found to increase generally with time as the separation distance decreased.

Distributed Buoyancy

Two relevant questions arise, such as: How critical is engine placement in achieving the effect shown in Fig. 5, and should the buoyancy caused by descent of the vortex pair in a stable atmosphere drive the vortices together? In order to investigate these questions, a second simulation was performed with the buoyant fluid initially distributed throughout the oval region of recirculation, as shown in Fig. 7, rather than being concentrated in the vortex cores. The total mass defect and total buoyant force, however, were kept the same as in the previous simulation; only their distributions were altered. The density

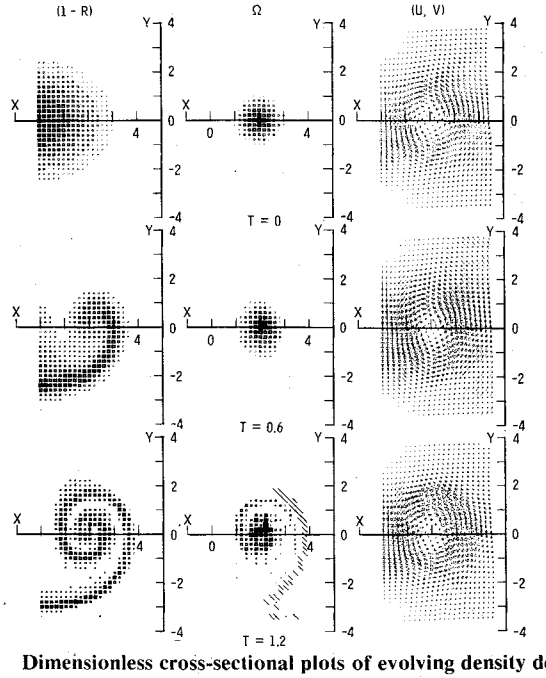

Fig. 7 Dimensionless cross-sectional plots of evolving density defect $1-R$, vorticity Ω, and velocity (U, V) for a wing-tip vortex with buoyant fluid distributed throughout the oval region of recirculation. Negative values of Ω are indicated by crosshatching. The stagnation point at the vortex center is shown to remain at $X=2$.

defect was taken to be a Gaussian function with elliptic contours corresponding to the oval of recirculation. Some of the buoyant fluid (in the Gaussian tail) is outside the oval and even beyond the grid boundaries. Therefore, the dimensionless mass defect M as, determined by numerical integration, is slightly less in Fig. 8 than in Fig. 6.

The simulation of Fig. 7 shows that, although the buoyant fluid wraps around the vortex, it does not converge on the vortex center. In fact, superposing the diagrams for Ω and $1-R$ shows that the vorticity and buoyant fluid do not mix (except for the buoyant fluid initially in the core); instead, they form interleaved spirals. Movies made by P.B. MacCready Jr. show that when helium-filled balloons are released below an airplane wake, they quickly go to the low-pressure centers of the wing-tip vortices. The simulation of Fig. 7 shows that this is not always true for distributed buoyant gas.

Figure 7 shows that the stagnation point at the vortex center remains at $X=2$ during the time period that the stagnation point in Fig. 5 drifted from $X=2$ to $X=1.4$. Distributed buoyancy, therefore, is not effective in driving wing-tip vortices together. Although not plotted in Fig. 8, the descent speed of the vortex pair was found to remain essentially constant for the duration of the computation.

Figure 8 shows that initially, the dimensionless circulation G of the right-hand vortex steadily decreases, while for the previous computation, Fig. 6 showed that G remained constant. An explanation for the behavior of G with time is found in the Bjerknes equation. Application of this equation of the right-hand semioval shows that if accelerations of the buoyant fluid are neglected, $d\Gamma/dT$ is negative when buoyant fluid spans across the symmetry plane, and $G=$const when no buoyant fluid is on the symmetry plane.

The downard dimensionless momentum Π of the vortex pair is given by

$$\Pi = 2GX_G \tag{4}$$

Because of the buoyant force, this downward momentum must decrease with time. Since the buoyant force is the same in both simulations, $d\Pi/dT$ must be equal for both. For the simulation shown in Figs. 5 and 6, the momentum decreased

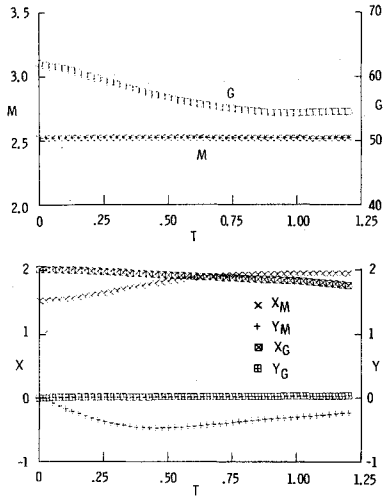

Fig. 8 Timewise variation of the dimensionless circulation G and mass defect M and of the coordinates of their centroids for the distributed buoyancy computation of Fig. 7.

through a decrease in the separation distance $2X_G$; for the simulation of Figs. 7 and 8, the momentum decreased at the same rate primarily through a decrease in G. Eventually in Figs. 7 and 8, as buoyant fluid is convected away from the symmetry plane, G becomes constant and X_G starts decreasing. Even then, however, the decrease in X_G is mainly due to generation of diffuse negative vorticity on the periphery of the oval, and movement of the stagnation point at the vortex center is still retarded.

These simulations have shown that if aircraft trailing vortices are to be driven together by buoyancy, the buoyant fluid should be injected directly into the vortex cores. For vortices made buoyant by jet engine exhaust, therefore, engine placement is very important. Placing the engines at the wing-tips and/or flap-tips would be effective in causing the vortices to drift together. Placement elsewhere may not be effective.

Conclusions

Wind-tunnel tests have demonstrated that buoyant fluid ejected downstream at a wing-tip or flap-tip will enter the core of the trailing vortex and cause it to drift horizontally in accordance with the theory presented by Costen.[1] These tests have also confirmed the results of previous experiments, that sufficiently high injection rates cause the vortices to undergo transition from small laminar cores to diffuse turbulent cores. The thrust of the injection jets for this transition was shown to be less than the induced drag of the wings tested. These results indicated that placing the propulsion engines of a jet aircraft at the wing-tips and flap-tips would help to alleviate the aircraft wake: 1) by causing the vortices from the two wings to drift toward each other as they descend and thus break up more quickly through the Crow or burst instability; and 2) by making the vortex cores more diffuse and turbulent.

Two-dimensional computer simulations showed that buoyant-core wing-tip vortices in near proximity continue to be driven together despite elongation of the cores parallel to the symmetry plane. They also showed that engine placement is critical if jet exhaust is to enter the cores and drive the vortices together. Distributed buoyancy resulting from general engine placement or from descent of the wake in a stable atmosphere will not promote this drift because the buoyant fluid, while wrapping around the vortices, does not converge on their cores.

References

[1] Costen, R.C., "Drift of Buoyant Wing-Tip Vortices," *Journal of Aircraft*, Vol. 9, June 1972, pp. 406-412.

[2] Crow, S.C., "Stability Theory for a Pair of Trailing Vortices," *AIAA Journal*, Vol. 8, Dec. 1970, pp. 1272-1279.

[3]Chevalier, H., "Flight Test Studies of the Formation of Trailing Vortices and a Method to Accelerate Vortex Dissipation," AIAA Paper 72-988, Palo Alto, Cal., 1972.

[4]Crow, S.C., *Panel Discussion: Aircraft Wake Turbulence and its Detection,* edited by J.H. Olsen, A. Goldburg, and M. Rogers, Plenum Press, 1971, pp. 577-593.

[5]Bilanin, A.J. and Widnall, S.E., "Aircraft Wake Dissipation by Sinusoidal Instability and Vortex Breakdown," AIAA Paper 73-107, Washington, D.C. 1973.

[6]Ciffone, D.L. and Orloff, K.L., "Far-Field Wake-Vortex Characteristics of Wings," *Journal of Aircraft,* Vol. 12, May 1975, pp. 464-470.

[7]Corsiglia, V.R., Rossow, V.J., and Ciffone, D.L., "Experimental Study of the Effect of Span Loading on Aircraft Wakes," *Journal of Aircraft,* to be published.

[8]Poppleton, E.D., "Effect of Air Injection Into the Core of a Trailing Vortex," *Journal of Aircraft,* Vol. 8, Aug. 1971, pp. 672-673.

[9]Mason, J.H., and Marchman, J.F., III, "Far-Field Structure of an Aircraft Trailing Vortex, Including Effects of Mass Injection," NASA CR-62078, April 1972.

[10]White, R.P., Jr. and Balcerak, J.C., "An Investigation of the Mixing of Linear and Swirling Flows," Report 72-04, Rochester Applied Science Associates, Inc., Rochester, N.Y.

[11]Patterson, J.C., Jr., "Lift-Induced Wing-Tip Vortex Attenuation," *Journal of Aircraft,* Vol. 12, Sept. 1975, pp. 745-749.

[12]Zalovcik, J.A. and Dunham, R.E. Jr., "Vortex Wake Research," AGARD Flight Mechanics Panel Symposium on Flight in Turbulence, Bedfordshire, Eng., May 1973.

[13]Pocklington, H.C., "The Configuration of a Pair of Equal and Opposite Hollow Straight Vortices of Finite Cross-Section Moving Steadily Thrugh Fluid," *Proceedings of the Cmbridge Philosophical Society,* Vol. 8, 1894, pp. 178-187.

[14]Lamb, H., *Hydrodynamics,* Sixth ed., Dover Publ., 1945.